ELECTROMAGNETICS

The role of probe attenuation in the TDR characterization of dielectrics

P. Savi and I.A. Maio
Dipartimento di Elettronica, Politecnico di Torino,
C.so Duca degli Abruzzi 24, 10129 Torino, Italy,
e-mail:patrizia.savi@polito.it.

S. Ferraris
Università degli Studi di Torino,
Dipartimento di Economia e Ingegneria Agraria, Forestale e Ambientale (D.E.I.A.F.A.),
Sezione di Idraulica Agraria,Via Leonardo da Vinci - 10095 - Grugliasco (TO).

Index Terms Time-domain reflectometry (TDR), inverse problems, dispersive dielectrics, soil permittivity.

Abstract

The influence of the measurement setup on the estimation of dielectric permittivity spectra from time-domain reflectometry (TDR) responses is investigated. The analysis is based on a simplified model of the TDR measurement setup, where an ideal voltage step is applied to an ideal transmission line that models the probe. The main result of this analysis is that the propagation in the probe has an inherent band limiting effect, and the estimation of the high-frequency permittivity parameters is well conditioned only if the wave attenuation for a round trip propagation in the dielectric sample is small. This is a general result, holding for most permittivity model and estimation scheme. It has been verified on real estimation problems by estimating the permittivity of liquid dielectrics and soil samples via an high-order model of the TDR setup and a parametric inversion approach.

I. INTRODUCTION

The Time-Domain Reflectometry (TDR) is a well-known measurement technique for the detection of discontinuites along the transmission paths of microwave and optical circuits. It has also been applied to a variety of problems such as high-precision level measurement systems (Gerding et al., 2006), and crack detection (Sun et al., 2009).

Recently, TDR has been widely applied in soil science, hydrology and agronomy to estimate the electrical properties of soils and to infer from them the soil water content and its salt concentration (Topp and Ferrè, 2002), (Robinson et al., 2003).

The two major features of TDR waveforms are the travel time and the 'late' time amplitude of the response: they are directly related to the apparent dielectric constant K_a and to the soil electrical conductivity γ. Still, more information on the dielectric properties of the soil can be obtained from the TDR waveforms. Therefore, interest has grown into the computation of the whole permittivity spectrum of soil samples from TDR responses (Heimovaara, 1994).

Owing to this application, over the past twenty years, great efforts have been spent on the design and testing of various type of probes (*e.g.,* (Robinson et al., 2005; Evett et al., 2006)); on the calibration of the TDR system, i.e. the relationship between the apparent dielectric permittivity and the soil water content (Topp et al., 1980; Roth et al., 1990; Hansson and Lundin, 2006), and on the methods to solve the inverse problem of estimating the permittivity from the

reflection responses (*e.g.,* see (Heimovaara, 1994; Oswald et al., 2006)).

In spite of the advances in the modeling of the TDR setup and in the evaluation of the permittivity from the TDR response, the intrinsic limitations introduced by the TDR measurement setup on the estimation of the permittivity spectrum has rarely been addressed. If the information on the electrical properties of the sample under test are lost due to the characteristics of the measurement system, it is not possible to retrieve such informations whatever the accuracy of the inversion method used. The aim of this paper is to analyze the limitations introduced by the TDR measurement setup and in particular the effect of the wave attenuation along the TDR probe. It will be shown that the length of the TDR probe puts an upper limit to the frequency and that this limit is independent on the well-known impact of the TDR instrument bandwidth (Lin, 2003; Huisman et al., 2004).

The study exploits a simplified model of the TDR measurement system, where an ideal voltage step is applied to an ideal cable connected to the probe. An equivalent circuit of the TDR measurement setup based on transmission line theory (Pozar, 1990) is introduced and a parametric representation of the permittivity spectrum as a one-pole real rational model (Debye's permittivity model) is assumed (Hasted, 1973). The limitations of the TDR measurement setup are then highlighted by means of a frequency domain analysis.

The reflection coefficient $S_{11}(j\omega)$ at the input port of the probe is written as a function of the model parameters in the frequency domain. The decomposition of S_{11} into a sequence of echoes and the analysis of the second echo network function points out the role of the probe attenuation and a threshold on the attenuation of the working condition of the measurement setup.

The role of the probe attenuation is then verified on some real cases (water, methanol, dry sand). To this end, a high-order model (in which the finite rise-time and the aberration of the real input signal, and the junction between the probe and the port of the TDR instrument are kept into account) and a *parametric inversion* approach for the permittivity evaluation are exploited.

II. TDR SIMPLIFIED MODEL AND PROBE ATTENUATION

Our laboratory TDR measurement system is composed of a matched step source (1), a scope detecting voltage (2), a coaxial cable (3), connectors and external cables (4), a coaxial probe to be filled with the dielectric under test (5) and a probe termination (6). Parts (1)-(3) are included in the TDR instrument, whereas parts (4)-(6) form the device whose reflection response is measured (see Fig. 1a). In order to point out the inherent properties of the TDR responses, we consider the simplified model shown in Fig. 2 where an ideal voltage step (infinite bandwidth) is applied to an ideal cable of characteristic admittance Y_o connected to the probe. The probe is an open-ended ideal coaxial line and can be modeled as a TEM transmission line of characteristic admittance and time delay of the empty line Y_a and τ_a, respectively. In this lossless, simplified model, the measured quantity is the time evolution of the backward wave at the probe input, *i.e.,* $r(t) = L^{-1}[S_{11}(s)(1/s)]$ where S_{11} is the reflection coefficient at the cable-probe discontinuity, $s = \sigma + j\omega$ is the Laplace variable, L^{-1} is the inverse Laplace transform operator, and lower-case and upper-case letters are used to indicate transform pairs. When the probe is filled by a dielectric with the relative permittivity $\epsilon_r(s)$, the S_{11} function is:

$$S_{11}(s) = \frac{\Gamma + \mathrm{P}^2}{1 + \Gamma\,\mathrm{P}^2} \tag{1}$$

where $\Gamma(s) = (Y_o - Y_a\sqrt{\epsilon_r(s)})/(Y_o + Y_a\sqrt{\epsilon_r(s)})$ is the partial reflection coefficient at the cable-probe discontinuity and $\mathrm{P}(s) = \exp(-s\tau_a\sqrt{\epsilon_r(s)})$ is the propagation factor along the probe.

The Debye's permittivity model is considered to describe the unknown permittivity:

$$\epsilon_r(s) = \epsilon_\infty + (\epsilon_s - \epsilon_\infty)/(1 + \frac{s}{\omega_{rel}}) \tag{2}$$

where ϵ_∞, ϵ_s, and $\omega_{rel} = 2\pi f_{rel}$ are the model parameters. Therefore, the measurement setup is described by five parameters (ϵ_s, ϵ_∞, ω_{rel}, Y_a, τ_a). To facilitate the analysis, the following normalized quantities are introduced:

$$\mathcal{T} = \tau_a\sqrt{\epsilon_\infty}\,\omega_{rel},\ \eta = \epsilon_s/\epsilon_\infty\ ,\mathcal{Y} = Y_a\sqrt{\epsilon_\infty}/Y_o \tag{3}$$

together with the normalized time $T = t\,\omega_{rel}$ and complex frequency $S = s/\omega_{rel}$, respectively. The analysis exploits the decomposition of the normalized reflection coefficient, $\bar{S}_{11}(S)$, into a

sequence of echoes:

$$\begin{aligned}\bar{S}_{11}(S) \;=\; & \bar{\Gamma}(S) + (1-\bar{\Gamma}^2(S))\,\bar{\mathrm{P}}^2(S) + \\ & (1-\bar{\Gamma}^2(S))\,(-\bar{\Gamma})\bar{\mathrm{P}}^4 + \ldots\end{aligned} \tag{4}$$

The partial reflection coefficient, $\bar{\Gamma}(S)$, and the propagation factor, $\bar{\mathrm{P}}(S)$, can be expressed as a function of the normalized quantities as follows:

$$\begin{aligned}\bar{\Gamma}(S) \;&= \frac{1-\mathcal{Y}\sqrt{\bar{\epsilon}}}{1+\mathcal{Y}\sqrt{\bar{\epsilon}}} \\ \bar{P}(S) \;&= e^{-\mathcal{T}S\sqrt{\bar{\epsilon}}}\end{aligned} \tag{5}$$

where $\mathcal{Y} = Y_a\sqrt{\epsilon_\infty}/Y_0$, and $\bar{\epsilon} = 1 + (\eta-1)/(1+S)$ and $S = j\Omega$, where Ω is the normalized angular frequency.

The first term of equation (4), $\bar{H}_1(S) = \bar{\Gamma}(S)$, is the network function relating the incident wave to the wave reflected by the cable-probe discontinuity. The second term, $\bar{H}_2(S) = (1-\bar{\Gamma}^2(S))\,\bar{\mathrm{P}}^2(S)$, relates the incident wave to the wave reflected by the probe load and so on. In the time domain, these terms start at $T = 0,\ 2\mathcal{T},\ 4\mathcal{T},\ ...$, and give rise to the echoes forming the observed response, *i.e.,* $\bar{r}(T) = \bar{r}_1(T) + \bar{r}_2(T) + ...$ In order to study the properties of the ideal model responses, it is convenient to focus on the second echo, because it is the simplest term containing information on both the probe-cable discontinuity and on the propagation in the dielectric. The behavior of the second echo is decided by the network functions $\bar{H}_2(S)$ and, in particular, by the square propagation factor $\bar{P}^2(S) = exp(-2\mathcal{T}S\sqrt{\bar{\epsilon}})$. Figure 3a,b shows $|\bar{P}^2(j\Omega)|$ for $\mathcal{T} = 6, 15, 40$ and $\eta = 1.5, 3$. (Panel b is a close-up view of the middle lower part of panel a). For growing $\mathcal{T}$ and η values, the high-frequency magnitude of $|\bar{P}^2|$ becomes negligibly small and, therefore, $\bar{H}_2$ becomes a bandlimited function. This bandlimiting effect is due to the imaginary part of $\bar{\epsilon}(j\Omega)$, that is responsible for the attenuation constant of $\bar{P}^2$:

$$\alpha = -\Re e\{j2\,\Omega\,\mathcal{T}\sqrt{\bar{\epsilon}(j\Omega)}\} = -2\,\Omega\,\mathcal{T}\,\Im m\Big\{\sqrt{1+\frac{\eta-1}{1+j\Omega}}\Big\} \tag{6}$$

The attenuation constant is plotted vs. frequency in Fig. 3c. Every attenuation curve is composed of a quadratic low-frequency part (the constant slope part in the bi-logarithmic scales of Fig. 3c) and by a constant high-frequency part. The constant part arises from the high frequency behavior

of $\Im m\{\sqrt{\bar{\epsilon}(j\Omega)}\}$, that is inversely proportional to Ω. The high-frequency asymptotic value of α is:

$$\lim_{\Omega\to\infty} \alpha(j\Omega) = \xi = \mathcal{T}(\eta - 1) \tag{7}$$

and the asymptotic value of $|\bar{P}^2|$ is $\exp(-\xi)$. For $\xi = 5$, the asymptotic value of $|\bar{P}^2|$ is close to 6.7×10^{-3} and can be considered small. The relation between the $|\bar{P}^2|$ and α curves of Fig. 3 is explained by this property. Bandlimited propagation factors are associated to attenuation curves with $\xi > 5$, and the propagation factors become small where their attenuation curves overpass the threshold level (see Fig. 3a,b,c).

In the following, we use the term low-attenuation (high-attenuation) to indicate measurement setups and TDR responses characterized by $\xi > 5$ ($\xi < 5$). Measurement setups working in high-attenuation conditions have $\bar{H}_2$ functions with small high frequency magnitudes. In these conditions, the network functions of the higher order echoes have small high-frequency magnitudes as well, because they include powers of the factor $\bar{P}^2$. As a consequence, in high-attenuation conditions, the high-frequency content of the measured TDR waveforms is low and their relation to the high-frequency permittivity spectrum is expected to be weak. According to this analysis, measurement setup operating in the low-attenuation domain are preferable.

As an example, consider the TDR waveforms corresponding to the low- and high-attenuation frequency responses shown in Fig. 4 with parameters $\epsilon_s = 12$, $\epsilon_\infty = 6$, $f_{rel} = 0.7\,\mathrm{GHz}$, $Z_a = \sqrt{\mathcal{L}/\mathcal{C}} = 77\,\Omega$, $\tau_a = 0.34\,\mathrm{ns}$ (low-attenuation, $\xi = 3.7$) and $\tau_a = 1\,\mathrm{ns}$ (high-attenuation, $\xi = 11$). When the wave reflected from the probe end has harmonic components with significant amplitude for frequency larger than f_{rel} the observed TDR waveforms are of low-attenuation type. This reflection behavior is illustrated in Fig. 4a, where the solid line curve is the magnitude of the network function of the first echo from the probe end for a low-attenuation case and the dotted straight line corresponds to the relaxation frequency (the bandwidth of the instrument source is larger than the relaxation frequency of the dielectric under test). Similarly, when the harmonic components of the wave reflected from the probe end have negligible amplitude for frequency larger than f_{rel}, the TDR waveform are of high-attenuation type (dashed curve of Fig. 4a). The bandwidth of the waveforms of high-attenuation type is therefore inherently limited to f_{rel}, regardless of the source bandwidth, and these waveforms are scarcely sensitive to the high-

frequency parameters of the permittivity. The two types of waveform can be easily identified because, in the low-attenuation waveform, the rising edge corresponding to the first echo from the probe end is asymmetric and steep, whereas, in the high-attenuation case, the edge is symmetric and gradual (see Fig. 4b, where $\rho(t) = 2v_o(t)/e_f - 1$, e_f asymptotic value of $e(t)$) for the transmission line model shown in Fig. 1b).

The low-attenuation condition can be expressed in physical parameters as:

$$\xi = \tau_a \omega_{rel} \frac{\epsilon_s - \epsilon_\infty}{\sqrt{\epsilon_\infty}} < 5 \tag{8}$$

or, equivalently, as:

$$2\tau_a \sqrt{\epsilon_\infty} < 10\, \epsilon_\infty / \omega_{rel}(\epsilon_s - \epsilon_\infty) \tag{9}$$

where $2\tau_a\sqrt{\epsilon_\infty}$ is the probe round trip delay. This means that $2\tau_a\sqrt{\epsilon_\infty}$, *i.e.,* the probe electrical length, must be limited in order to obtain low-attenuation operation.

As a consequence of (9), two limitations on the instrument resolution and on the length of the probe should be taken into account. The instrument resolution must be significantly finer than $10\,\epsilon_\infty/\omega_{rel}(\epsilon_s - \epsilon_\infty)$. In practice, the resolution of TDR instruments is limited by the rise time of their sources that is on the order of $150 \div 200\,\mathrm{ps}$ for conventional field instruments and of $30\,\mathrm{ps}$ for high-end instruments, and low attenuation measurements can be obtained only for dielectric with $\omega_{rel}(\epsilon_s - \epsilon_\infty)/\epsilon_\infty$ small enough. On the other hand, a too short probe ($l = \tau_a c$) cannot be considered both for practical reasons and because the transmission line model requires the cross-section to be much smaller than the length of the probe.

Some examples of parameter values are listed in Tab. 1. The ethanol can be considered as a limit case. In fact, the maximum round trip delay is $445\,\mathrm{ps}$ and can be detected by a standard TDR instrument, and the length of the probe in this case should be $3\,\mathrm{cm}$.

III. RESULTS

In this Section, the role of the probe attenuation and the type of attenuation condition (low or high) are investigated on some cases of practical interest.

To this end, the high-order model defined by the chain network of Fig. 1b is considered. In this model, the TDR source (part (1) of Fig. 1a) is represented by a matched source driving the network with the same waveform measured in the actual TDR instrument. The model source, therefore, takes into account the finite rise time and the aberration of the real input signal. The two-port element corresponding to part (4) of Fig. 1 takes into account the distortion effects due to the connector of the probe. The two-port element has been identified by fitting the response of the chain network to the response measured with the probe left empty (part 5). The unknown permittivity is assumed to be represented by Debye's relation modified in order to keep into account the conductivity γ of the dielectric under test:

$$\tilde{\epsilon}_r(s) = \epsilon_\infty + (\epsilon_s - \epsilon_\infty)/(1 + \frac{s}{\omega_{rel}}) + \frac{\gamma}{j\omega} \tag{10}$$

The four parameters $(\epsilon_s, \epsilon_\infty, \omega_{rel}, \gamma)$ of eq. (10) are estimated by a parametric inversion approach, i.e. by fitting the high-order model response to the measured one.

We consider the results shown in Fig. 5 for two reference liquids: water and methanol. The solid line curves are the measurements obtained by a HP 54120B digitalizing oscilloscope rise time 10ps, and a coaxial probe (Maury Microwave Airline, model no. 2653S10, $\ell = 10.5\,\mathrm{cm}$, shield and inner conductor radii $3.5\,\mathrm{mm}$ and $1.5\,\mathrm{mm}$, respectively, dc-resistance of inner conductor $9.4\,\mathrm{m}\Omega/\,\mathrm{m}$). A $50\,\Omega$ load is used to terminate the probe. The dashed line curves of Fig. 5 are obtained by using the Debye's permittivity representation (10) and by fitting the response of the high-order model to the measured curves. The TDR waveform of these examples is of the high-attenuation type due to a rising edge corresponding to the first echo from the probe that is symmetric. This is confirmed by the estimation procedure in which the sensitivity of the response to the high-frequency parameters (ϵ_∞ and f_{rel}) is weak. For these examples, only the low-frequency parameters (ϵ_s, γ) can be obtained. The best fit of the measured responses is obtained for $\epsilon_s = 78$, $\gamma = 0.3\,\mathrm{mS/m}$ for water (Lide, 1992), and $\epsilon_s = 32$, $\gamma = 0.1\,\mathrm{mS/m}$ for methanol (Weerts et al., 2001).

In the third example, we apply the parametric inversion procedure to the TDR response of a 3.4% volumetric water content dry sand sample. The TDR response shown in Fig. 6 (solid line) has been obtained with a Tektronix 1502B reflectometer (horizontal setting $0.1\,\mathrm{m}$ per division and a propagation velocity setting of 0.99) and the same coaxial probe of the previous example

(Maury Microwave Airline, model no. 2653S10) A $50\,\Omega$ load was used to terminate the probe and a 13-bit data acquisition is exploited (range from 0 to 8192). The TDR response of this example is a low-attenuation waveform and, according to the analysis of the previous Section, its estimation problem is expected to be well conditioned for the high-frequency part of the permittivity, too. The model response that best fits the measured curve is shown in Fig. 6 (dashed line) and the estimated values of the permittivity parameters are: $\epsilon_s = 3.18$, $\epsilon_\infty = 2.69$, $f_{rel} = 413\,\text{MHz}$ and $\gamma = 6.36 \cdot 10^{-4}\,\text{S/m}$. These parameter values correspond to $\xi = 0.28$, confirming that the measured response is of low-attenuation type, as expected.

The condition of the estimation problem is decided by the behavior of the error function around the estimated parameter values. An indicator of this behavior can be obtained by plots of the function over planes of the parameter space. The error function of this example over the plane $(\epsilon_\infty, f_{rel})$ is shown in Fig. 7 and looks as a well behaved convex surface, thereby suggesting the good condition of the estimation of the high-frequency parameters.

The examples of this Section confirm that the attenuation regime of the measured waveforms can be effectively predicted from their shape and that low-attenuation setup leads to well-conditioned estimation problem.

IV. CONCLUSION

The role of probe attenuation in the estimation of the dielectric permittivity spectrum from TDR waveforms has been studied. The analysis is based on an idealized model of the measurement setup and on Debye's model of the unknown permittivity. The main result is that two types of TDR waveforms (low-attenuation and high-attenuation) can be identified. The transition between the two types of waveforms is controlled by the wave attenuation along the probe. Low-attenuation operation can be obtained by using short probes and yields waveforms that are more sensitive to the high-frequency behavior of the permittivity, since their harmonic content extends beyond the relaxation frequency f_{rel}. Measurements on liquid dielectrics and sand samples confirm the prediction of the idealized model.

REFERENCES

Evett, S.R., J.A. Tolk, and T.A. Howell. 2006. Soil profile water content determination: Sensor accuracy, axial response, calibration, temperature dependence, and precision. *Vadose Zone J.*, 5:894–907.

Feng, W., C.P. Lin, R.J. Deschamps, and V. P. Drnevich. 1999. Theoretical model of multisection tdr measurement system. *Water Resour. Res.*, 35:2321–2331.

Gerding, M., T. Musch, and B. Schiek. 2006. A novel approach for a high-precision multitarget-level measurement system based on time-domain reflectometry. *IEEE Trans. on Microwave Theory and Techniques*, 54:2768–2773.

Hansson, K. and L.-C. Lundin. 2006. Water content reflectometer application to construction materials and its relation to time domain reflectometry. *Vadose Zone J.*, 5:459:468.

Hasted, J.B., 1973. *Aqueous Dielectric*. Chapman and Hall. London.

Heimovaara, T.J., 1994. Frequency domain analysis of time domain reflectometry waveforms 1. measurements of the complex dielectric permittivity of soil. *Water Resour. Res.*, 30:189–199.

Huisman, J.A, W. Bouten, J.A. Vrugt, and P.A. Ferré. 2004. Accuracy of frequency domain analysis scenarios for the determination of complex dielectric permittivity. *Water Resour. Res.*, 40.

Lide, D.R., 1992. *Handbook of chemistry and physics*. 73rd ed. CRC Press, London.

Lin, C.-P., 2003. Analysis of nonuniform and dispersive time domain reflectometry measurement systems with application to the dielectric spectroscopy of soils. *Water Resour. Res.*, 39:6–11.

Oswald, B., J. Doetsch, and K. Roth. 2006. A new computational techniques for processing transmission-line measurements to determine dispersive dielectric properties. *Geophysiscs*, 71:k31–k35.

Pozar, D.M., 1990. *Microwave Engineering*. Addison Wesley.

Robinson, D.A., S.B. Jones, J.M. Wraith, D. Or, and S.P. Friedman. 2003. A review of advances in dielectric and electrical conductivity measurement in soils using time domain reflectometry, *Vadose Zone J.*, special section - advances in measurement and monitoring. *Vadose Zone J.*, 2:444–475.

Robinson, D.A., M.G. Schaap, D. Or, and S.B. Jones. 2005. On the effective measurement frequency of time domain reflectometry in dispersive and nonconductive dielectric materials.

Water Resour. Res., 41:1–9.

Roth, K., R. Schulin, H. Fluhler, and W. Attinger. 1990. Calibration of time domain reflectometry for water content measurement using a composite dielectric approach. *Water Resour. Res.*, 10:22672273.

Sun, S., D.J. Pommerenke, J.L. Drewniak, G. Chen Liang Xue, M.A. Brower, and M.Y. Koledintseva. 2009. A novel tdr-based coaxial cable sensor for crack/strain sensing in reinforced concrete structures. *IEEE Trans. on Instrumentation and Measurements*, 58:2714–2725.

Topp, G.C. and P.-A. Ferrè. 2002. Water content, in methods of soil analysis, part 4, physical methods. *Soil Sci.Soc. of Am.*, 5:417–446.

Topp, G.C., J.L. Davis, and P. Annan. 1980. Electromagnetic determination of soil water content: Measurements in coaxial transmission lines. *Water Resour. Res.*, 16:574–582.

Weerts, A.H., J.A. Huisman, and W. Bouten. 2001. Information content of time domain reflectometry waveforms. *Water Resour. Res.*, 37:1291–1299.

Table captions:

Table. 1 Debye's parameter values for some typical dielectrics. $10\epsilon_\infty/\omega_{rel}(\epsilon_s - \epsilon_\infty)$ is the maximum round trip delay for low-attenuation operation.

Figure captions:

Fig. 1 TDR setup model exploited for permittivity estimation via waveform fitting (see Sec. III).

Fig. 2 Ideal model of a TDR measurement system.

Fig. 3 Magnitude of the propagation factor P (panels a and b) and attenuation constant α (panel c) versus normalized angular frequency Ω for $\mathcal{T} = 6, 15, 40$, and $\epsilon = 1.5, 3$. Panel b is a close-up view of panel a. The dashed horizontal lines of panel b and c indicate the threshold level $|\bar{P}^2| = \exp(-5)$ and $\xi = 5$, respectively.

Fig. 4 Panel a : magnitude of the network function of the first echo from the probe end for a low-attenuation case (solid line) and an high-attenuation case (dashed line). Panel b: TDR waveforms corresponding to the response of panel a. $\rho(t) = 2v_o(t)/e_f - 1$, e_f asymptotic value of $e(t)$ for the transmission line model shown in Fig. 1b. Dashed line: low-attenuation, $\tau_a = 0.34\,\text{ns}$ and $\xi = 3.7$. Solid line: high-attenuation, $\tau_a = 1\,\text{ns}$ and $\xi = 11$. Parameter values: $\epsilon_s = 12$, $\epsilon_\infty = 6$, $f_{rel} = 0.7\,\text{GHz}$, $Z_a = \sqrt{\mathcal{L}/\mathcal{C}} = 77\,\Omega$, $\tau_a = 0.34\,\text{ns}$ (low-attenuation, $\xi = 3.7$) and $\tau_a = 1\,\text{ns}$ (high-attenuation, $\xi = 11$). The responses of this figure hold for an ideal step input.

Fig. 5 Measured (solid lines) and simulated (dashed lines) TDR waveforms (*i.e.,* $\rho(t) = 2v_o(t)/e_f - 1$, e_f asymptotic value of $e(t)$) for the setup of Fig. 1b.

Fig. 6 Measured TDR response ($\rho(t) = 2v_o(t)/e_f - 1$, e_f asymptotic value of $e(t)$) for the setup of Fig. 1b) for a dry sand sample (solid line) and the best fit response of the model of this paper (dashed line). Model fitted parameters: $\epsilon_s = 3.18$, $\epsilon_\infty = 2.69$, $f_{rel} = 413\,\text{MHz}$, and $\gamma = 6.36 \cdot 10^{-4}\,\text{S/m}$, corresponding to $\xi = 0.28$.

Fig. 7 Error surface in the $(\epsilon_\infty, f_{rel})$ plane for the TDR response of Fig. 6.

Medium	f_{rel}	ϵ_s	ϵ_∞	$10\epsilon_\infty/\omega_{rel}(\epsilon_s - \epsilon_\infty)$	ref.
deionized water	17 GHz	80	4.22	5.2ps	(Heimovaara, 1994)
wet sand	7 GHz	15	3	57ps	(Feng et al., 1999)
ethanol	0.782 GHz	25.2	4.52	445ps	(Heimovaara, 1994)
dry sand	7 GHz	3	2.8	5.25ns	(Feng et al., 1999)

Table 1

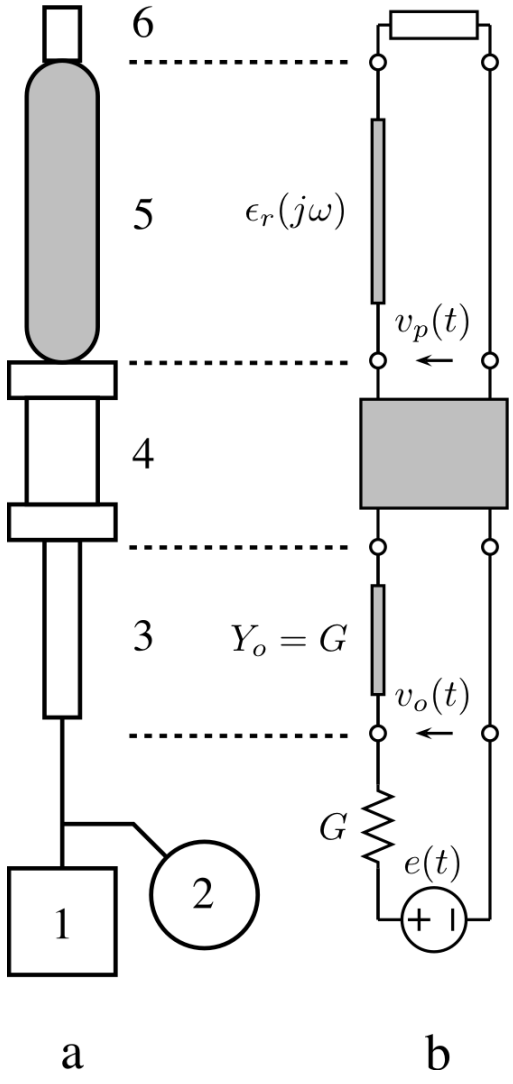

Figure 1

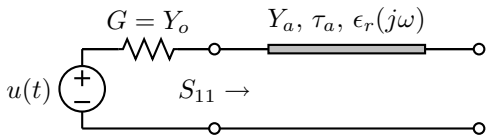

Figure 2

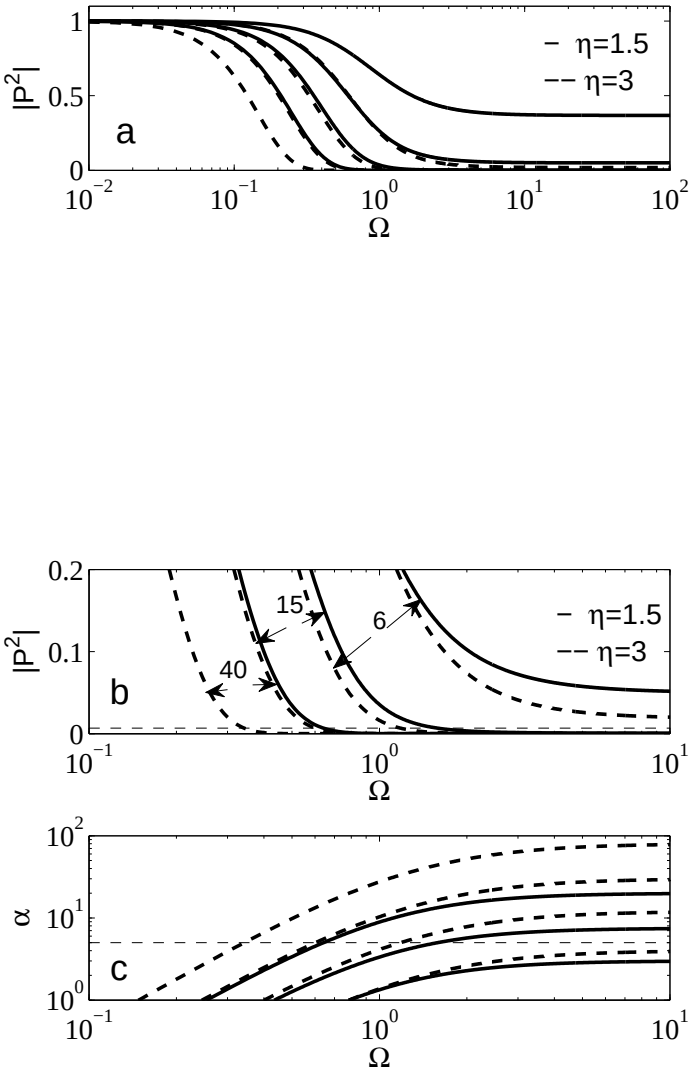

Figure 3

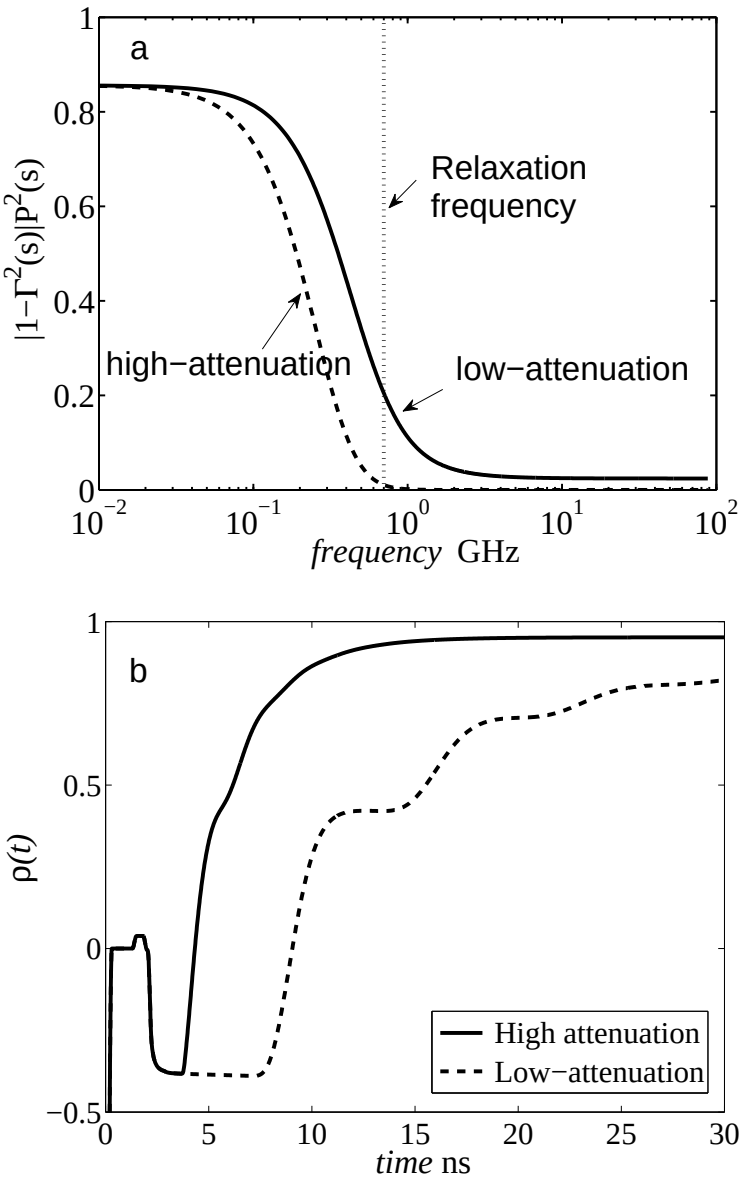
a
Relaxation
frequency
high−attenuation
low−attenuation
$|1-\Gamma^2(s)|P^2(s)$
frequency GHz
b
High attenuation
Low−attenuation
ρ(t)
time ns

Figure 4

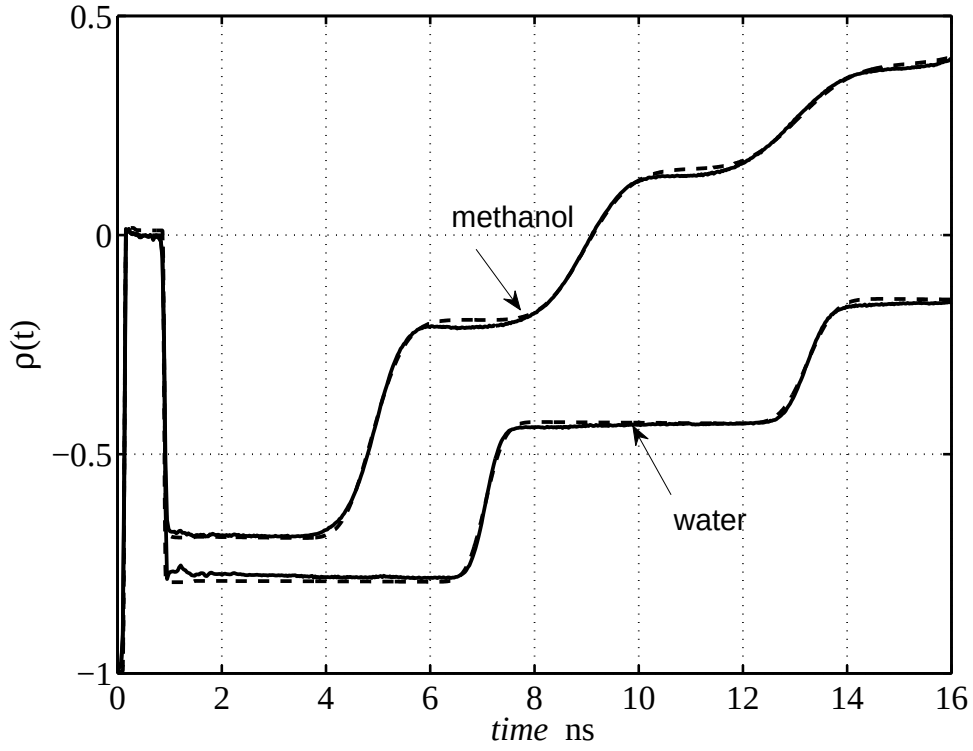

Figure 5

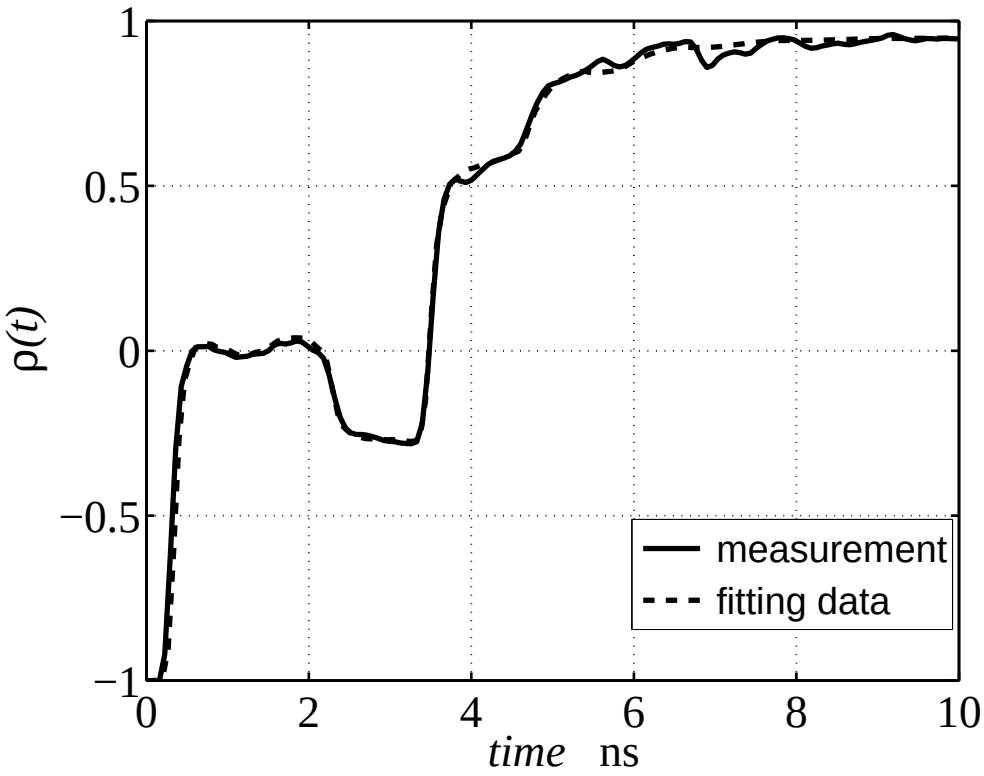

Figure 6

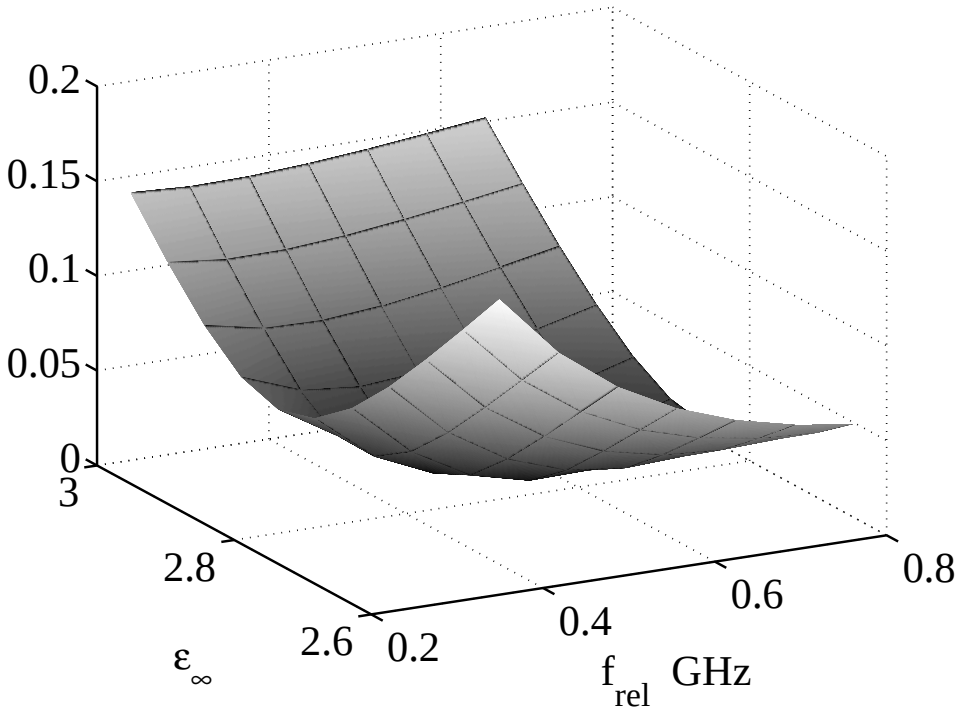

Figure 7